3
Experimental Details

The commonly used synthesis techniques for microwave absorbing materials have been discussed and summarized in chapter 2. In the present thesis work, the synthesis routes for preparation of such materials have been developed to cater the need for large scale production of bulk materials with reproducible MW absorption properties. In the section 3.1 various methods like gel to carbonate precipitation route, wet chemical polymerization of metal nanocomposite followed by pyrolysis, solid state precursor route and sol-gel route, used to synthesize the materials for the thesis work, have been discussed in detail. This includes the preparation of spinel /hexagonal phase ferrites, core-shell Ni nanoparticles, $BaTiO_3$ and $BiFeO_3$ materials for MW absorption application. The bulk powders are characterized for their structural, chemical, magnetic, morphological and microwave absorption properties using various characterization tools as described in section 3.2. Further, the selected materials having optimal MW absorption properties were processed with NBR for their composite preparation with different filler loading in wt% using rubber processing units viz. Two Roll Mixing Mill (TRMM) and High Temperature Compression and Moulding Press (HTCMP) as described in section 3.3. MW absorption properties of different rubber composites were evaluated using vector network analyzer (VNA) in desired MW frequency bands.

3.1 BULK MATERIALS PREPARATION TECHNIQUES

3.1.1 Gel to Carbonate Precipitation Route (Spinel and hexagonal ferrite powders)

Wet chemical synthesis through gel to crystalline conversion route and gel to carbonate route for ultrafine ceramic powders continue to be the subject of intense research activity as the materials synthesized using these processes exhibit advantages over powders derived from conversion routes. In the present work, gel to carbonate route has been adopted for the preparation of ultrafine particles of ferrites, which can be easily scaled for large scale synthesis of the desired material. The flow chart of this route is shown in Figure 3.1. In this method, the co-precipitations of divalent cations as fine particles of carbonate within hydrated gels of ferric hydroxide is carried out by the adding the ammonium hydroxide or sodium carbonate to the mixed solutions of ferric chloride and one or more of the transition metal ions as per stoichiometric compositions. Such co-precipitation is possible because of the instability of the carbonate and oxycarbonate of iron (Fe) in an aqueous media in comparison to the polymerized hydroxide; whereas, strontium carbonate is readily precipitated within the voluminous ferric hydroxide gel. The method produces composites powders with submicron crystalline particles of the carbonates, embedded within the amorphous medium of $Fe_2O_3.xH_2O$ ($70<x<110$). The collected precipitate is first dried in an air oven and then calcined at different temperatures. Subsequently, upon heating at elevated temperature (~650°C) for 3h, the reaction between carbonates and amorphous ferric oxide xerogel takes place, causing the formation of hexaferrites. However, further sequential annealing at higher temperatures (~950°C and 1250°C for 3h each) leads to the micron size particles with desirable MW absorption properties. By suitably adjusting the compositions of strontium, divalent transition metals or of ferric ions, the composites of spinel ferrites and hexaferrites can be realized. Furthermore, in the absence of strontium, this procedure yields only the spinel ferrites. By following the above procedure, M-phase, Y-phase, W-phase,

and X-phase hexaferrites are realized by taking divalent metal cations such as Co, Ti, Ni, Mn and Zn during the synthesis process.

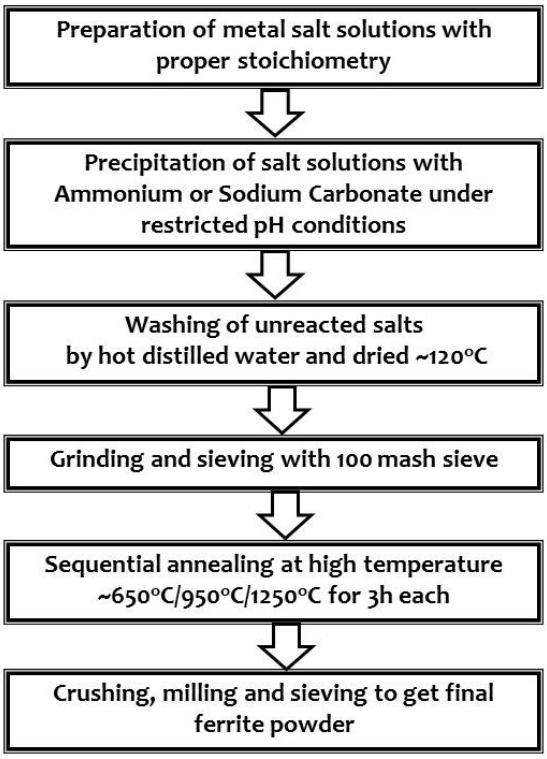

Figure 3.1: Process flow chart for gel to carbonate precipitation route followed by sequential annealing

Among different ferrites, the Z-type hexaferrite is considered to be the difficult to prepare crystallographically phase pure. In the present work, synthesis process has been optimized, where the sequential annealing cycles are developed to get the desired crystallographic M, Z and W-phases or composite mixed phases.

3.1.2 Wet Chemical Synthesis of Polymer Nanocomposites Followed by Pyrolysis

In the present thesis work, a previously established synthesis process by Vadera *et al*. [Vadera *et al*., 1997] has been adopted for in-situ preparation of metal oxide nanocomposites in the co-polymer matrix. Further, to get the metal nanoparticles, pyrolytic decomposition of prepared nanocomposites has been carried out in the inert nitrogen ambient at elevated temperatures. The burnet polymer converts into amorphous carbon/graphite as shell materials in conjunction with nano-metallic core. The details about these two step process are described below.

3.1.2.1 Synthesis of Metal Oxide Nanocomposites in Copolymer Matrix

In this synthesis process, the addition of Anilne to distilled water leads to the formation of a co-polymer by using aniline and concentrated HCl as the precursors. Further, formaldehyde is added to the mixture. The reaction advances through the formation of para-amino-benzyl alcohol, followed by the condensation of the amino and hydroxyl functional groups. Due to the exothermic nature of the reaction, the large amount of heat is released, necessitate the cooling down of the solution to room temperature. At the same time, salt solution is made by dissolving of metal halide in the water. In the next step, the salt solution is added to the co-polymer solution under continuous stirring. The stirred solution is kept about ~ 45 - 60 minutes for the completion of reaction. The reaction mixture was washed several times using hot distilled water to remove the alkali ions and filtered. The obtained filtered powder was dried and crushed to get the desired metal nanocomposite powder.

3.1.2.2 Synthesis of Core-Shell Metal Nanoparticles

The metal nanoparticles constitute one of the most important research domains due to their potential in wide areas of science and technology. The previous studies by Vadera *et al.* have established that the metal oxide nanocomposites pyrolysed in an inert atmosphere lead to formation of metal/metal alloys. This observation has been used to synthesize a number of nanoparticles of metal and metal alloys systems. In a typical synthesis process, nanocomposite powder of metal oxide is filled in a sample holder, made of quartz, and fixed in the tubular furnace. Initially, high purity N_2 (>99%) is flushed in reactor tube for ~10 minutes to get the inert ambient. The temperature of furnace was raised at the rate of 8°C/min in the range of 550°C-850°C for 1h under continuous flow of N_2 gas for decomposing nanocomposites into the desired geometrical structures. The finally prepared powder was collected from quartz tube after cooling down the furnace to room temperature. Thus, the final product is carbon/graphite coated metal/metal alloy nanoparticles. Complete synthesis scheme is summarized in Figure 3.2 as shown below.

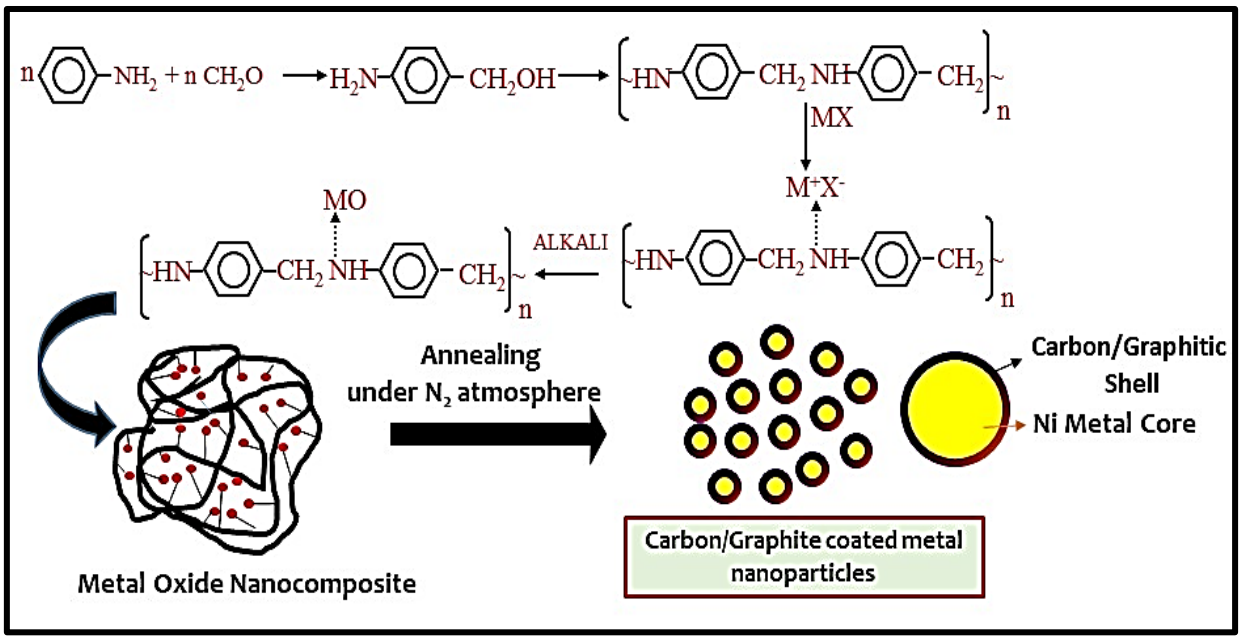

Figure 3.2: Process flow chart for synthesis of graphite coated core-shell metal nanoparticles

3.1.3 Sol-Gel Synthesis Route ($BiFeO_3$ Multiferroics)

$BiFeO_3$ powder samples are prepared using sol-gel synthesis technique. The sequential flow of chemical selection and their dissolution is explained in the synthesis block diagram, Fig. 3.3. First, twice the molarity of bismuth or iron molar solution was considered for glycine and prepared in 50ml of ethanol. After the homogeneous mixing of glycine in ethanol, the stoichiometric equimolar ratio of bismuth nitrate and iron nitrate are dissolved in glycinated ethanol solution and small amount of nitric acid was added to dissolve chemical reagents completely, as mentioned in synthesis flow chart, Figure 3.3. The dissolved mixture was under constant magnetic stirring for homogenous mixing.

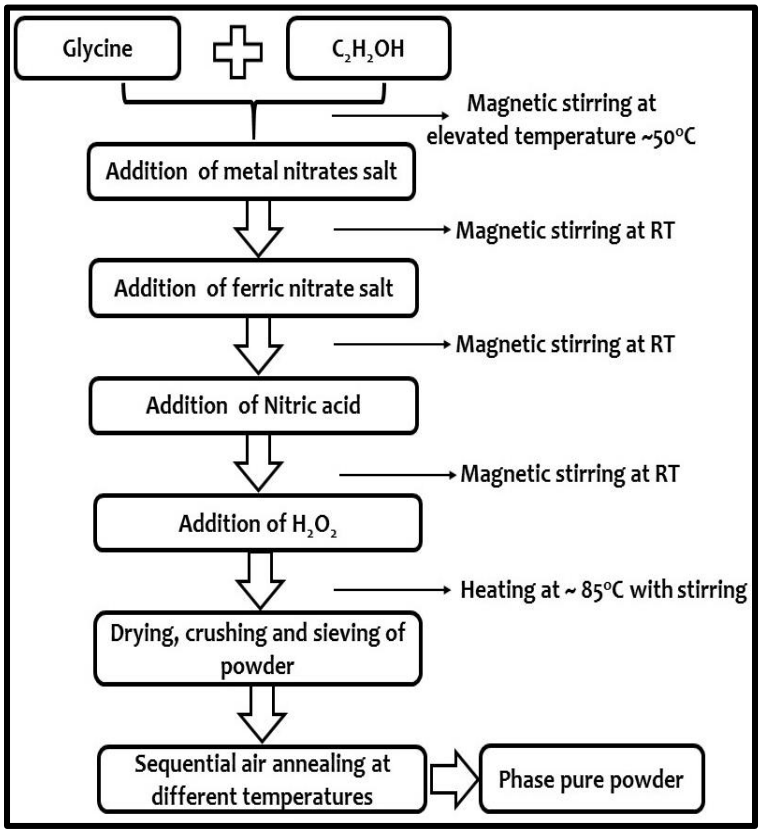

Figure 3.3: Process flow chart for sol-gel synthesis route

3.1.4 Solid State Synthesis (Tetragonal $BaTiO_3$ Ferroelectrics)

The solid state precursor route is the most common synthesis route for the preparation of ceramics materials due to its simplicity and easy processing. The process involves solid state reaction among mechanically activated precursors in high temperature conditions resulting into the desired final material. The first and foremost condition is to select the precursors, which are preferably reactive in nature to facilitate the interaction among materials. For the same reason oxides and carbonates based precursors were selected in the present thesis work. In the next step, mechanical activation of raw precursor powders was done by mechanical milling, using analytical/planetary mill to enhance the surface area of powder for assisting the solid state reaction among them. In the present study, analytical mill (make: IKA) has been used for initial milling of individual raw precursors at 15 minutes at 20,000 rotations per minutes (rpm). All the mechanically activated precursor powders were further homogenized using analytical mill for 10 minutes at 10,000 rpm. The solid mixtures of these precursors were transferred into alumina crucible and sequentially annealed at different temperatures in the range of 700-1100°C. The annealed powder was further crushed using pestle-mortar and sieved through 100 mash size (~ 149 μm). The prepared powder was characterized for its structural, chemical, morphological and EM studies. The typical solid state synthetic route optimized in the present thesis work is depicted in process flow chart, Figure 3.4.

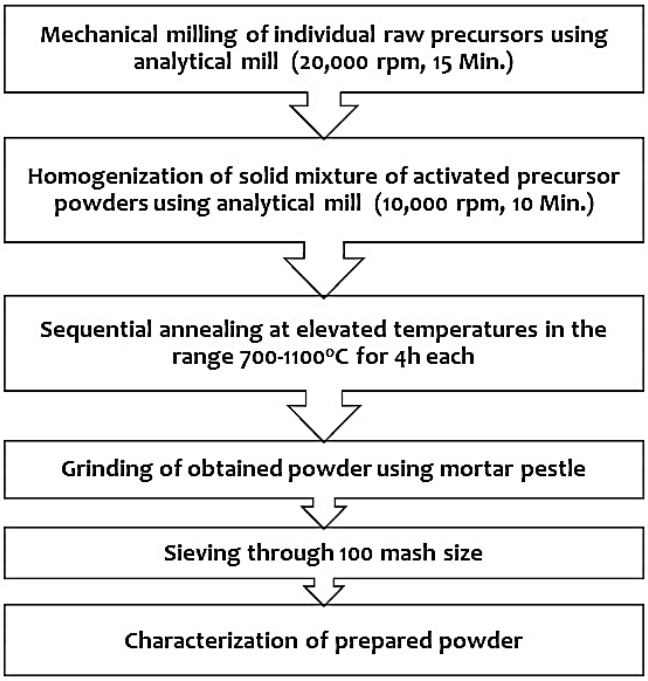

Figure 3.4: Process flow chart for solid state synthesis of ferroelectric ceramics

3.2 PREPARATION OF RUBBER BASED COMPOSITES

The functional filler powders with optimal MW absorption was selected as the filler material and impregnated in a suitable rubber matrix. Acrylonitrile Butadiene Rubber (NBR) has been chosen as a base matrix since it has good mechanical strength, and ease of fabricating rubber sheets. Rubber based microwave absorbing sheet was fabricated using Two Roll Mixing Mill (TRMM) and High Temperature Compression Moulding Press (HTCMP), shown in Figure 3.5(a)-(b). The TRMM consist of two identical cylindrical rolls in horizontal position rotating in opposite direction. The repetitive mastication of rubber in narrow gap of these cylinders provides uniform mixing of fillers in rubber matrix [Gupta, 1998]. Different additives were mixed in the compound for vulcanization and curing of rubber compound in parts per hundred (PHR) of rubber. The additives include sulphur (2 PHR) as vulcanizing agent, Mercapto-Benzo-Thiazol-Di-sulphite MBTS (1.5 PHR) as accelerator for curing of rubber-filler compound, ZnO (5 PHR) & Stearic Acid (2 PHR) as activator to enhance the effect of accelerator and Tri-methyl-Di-Qunoline TDQ (1 PHR) as antioxidant for rubber system to prevent it from degradation [Barlow, 1993]. Functional filler material at different wt% ratio were loaded in rubber matrix to fabricate the rubber-filler composite matrix. After homogeneous mixing of compound in mixing mill, the compound was placed in a 30 mm x 30 mm x 3 mm (LxBxD) size mould. This mould was hydraulically pressed with 30 Ton pressure at 160°C for 20 Minutes, as shown in Figure 3.5(b). After completion of this compaction cycle, the mould was cooled to ambient temperature and rubber sheet was collected for MW characterization.

Table 3.1 : List of additives used in rubber processing

S. No.	Ingredients	PHR of Rubber	Specifications
1	NBR (Nitrile Butadiene Rubber)	100	(ACN 28-35%)
2	Accinox TQ (Quinoline Type Anti-oxidant)	1.0	Specific Gravity: 1.08
3	Zinc Oxide	5.0	As per IS: 3399
4	Stearic Acid	2.0	As per IS : 1676
5	MBTS (Mercapto BenzThiazole Disulphide)	1.5	As per IS : 8483
6	Tri-methyl-Di-Qunoline TDQ	1.0	As per IS : 8979
7	Sulphur	1.0	As per IS : 8851

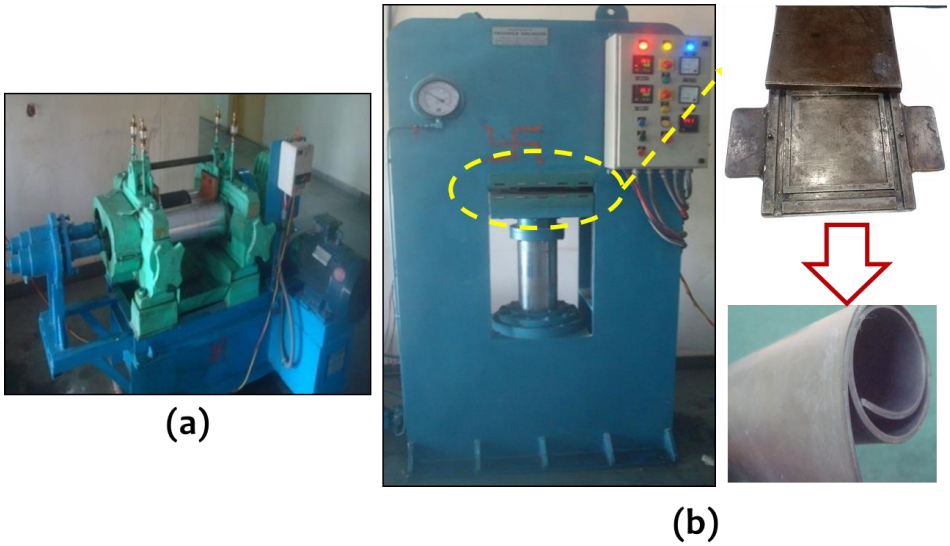

Figure 3.5: (a) Two roll mixing mill (b) Pressing of rubber sheets using high temperature compression moulding press, mould for pressing and fabricated flexible rubber sheet

3.3 SAMPLE CHARACTERIZATION TECHNIQUES

Investigation of structural, chemical, optical, magnetic, morphological and functional properties of the synthesized bulk and nanostructured materials is essential to determine the structure, property and process correlation for understanding the MW absorption characteristics. Several techniques viz. X-ray diffraction (XRD), Fourier transform infrared (FTIR), vibrating sample magnetometer (VSM), scanning electron microscope (SEM), energy dispersive X-ray (EDX), high resolution transmission electron microscope (HRTEM), UV-Vis spectrophotometer, Raman vibrational spectroscopy, Superconducting Quantum Interference Device (SQUID) magnetometer and Vector Network Analyzer (VNA) were used to determine these properties Further, rubber composites, fabricated using identified materials, were evaluated for their MW absorption properties using MW characterization techniques. In this section the details of equipment used for each characterization, their basic principle and methods for measurements are discussed.

3.3.1 Powder X-ray Diffraction (XRD) Method

The crystal phase, crystal structure, lattice parameters and particle sizes have been determined by the powder X-ray diffraction (XRD) technique [Cullity, 1956] using PANalytical X'pert Pro diffractometer instrument with Cu X-ray source of wavelength 1.54A°. A schematic drawing of the instrumental set-up is shown in Figure 3.6 (a). A typical powder XRD instrument consists of four main components as (i) X-ray source (X) and collimation assembly (A) (ii) Sample mounting assembly (B) (iii) Receiving optics; slit (C) and exit beam monochromator (D), and (iv) Detector assembly (E). The angle between the plane of the specimen and the X-ray source is θ, known as Bragg angle. However, the X-ray intensities are measured at 2θ position, which is angle between incident X-ray and detector assembly, as shown in Figure 3.6 (a). When a beam of X-ray is incident on the sample, these are diffracted by crystal atoms, arranged in the lattice planes of a particular phase of the material. If the diffracted beams are in phase, they interfere constructively and the diffracted intensity becomes the maximum at that particular angle. The Bragg's law establish a relation between the diffracted X-ray wavelength (λ), the inter-planar spacing (d_{hkl}) and the angle of diffraction (θ), as given below in Eq. (3.1) [Bragg, 1913]

$$2d_{hkl}\,\mathrm{Sin}\,\theta = n\lambda. \qquad (3.1)$$

For the first order diffraction, n=1 and by knowing the values θ and λ, we can calculate the d_{hkl} value for a particular plane for (h k l) miller indices. The XRD spectra are recorded with diffraction peaks of varying intensity at different 2θ positions. The peak position and intensity

are determined by the crystal symmetry and atomic arrangement at crystal lattice sites. The identification of crystal structure is done by indexing of crystal peaks with respective miller plane with available database in form of ICDD cards or by analytical methods. The shifting of XRD peaks in comparison to standard position is attributed to lattice strain in the crystal. Nanomaterials have characteristics of broadening of XRD peaks due to their finite size effect. The size of materials up to the limit of ~100nm, can be estimated with the help of Debye-Scherrer relation given below in Eq. (3.2)

$$d = \frac{K\lambda}{B\,\mathrm{Cos}\theta} \tag{3.2}$$

Where d is the average particle size, λ is the X-ray wavelength, θ is the Bragg angle, K is constant ~0.89 and B is the peak broadening in terms of full width at half maxima (FWHM). In the present thesis work, the lattice parameter (a) were calculated for cubic crystal structure with the obtained miller indices (h k l) and inter-planar spacing (d) by XRD spectra using the Eq. (3.3) [Pecharsky and Zavalij, 2003]

$$d = \frac{a}{\sqrt{h^2+k^2+l^2}} \tag{3.3}$$

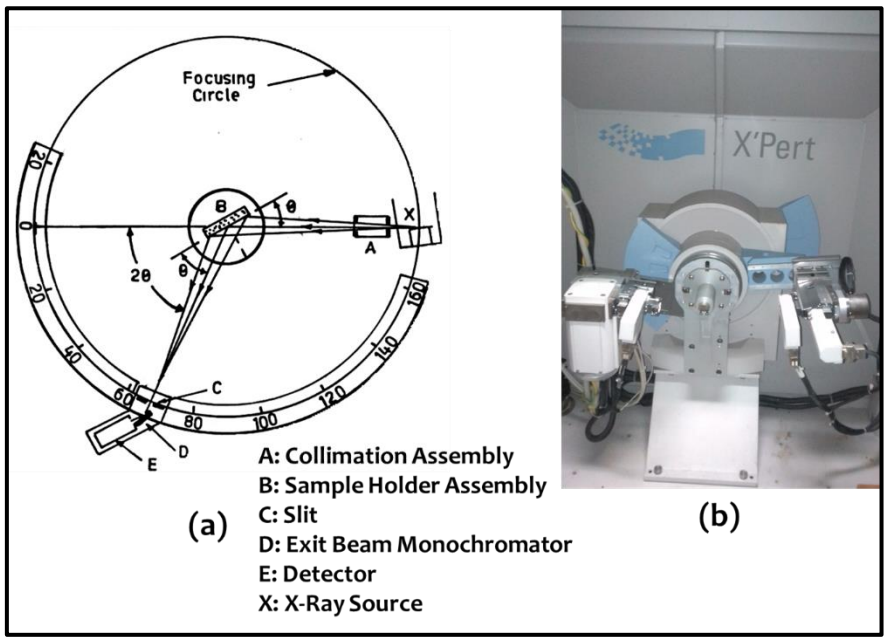

Figure 3.6: (a) Schematic for of geometrical arrangement of X-ray diffractometer (Source: Cullity, 1956) (b) PANalytical X'pert Pro diffractometer instrument used for XRD studies

3.3.2 Fourier Transform Infra-Red (FTIR) Spectroscopy

FTIR spectroscopy is an important and popular tool for identification of functional groups present in the chemical compounds. It is based on the absorption measurement of different IR frequencies corresponding to the characteristic vibrational frequency of a chemical bond [Brain, 1978; Bellamy, 1986]. The vibrational frequency is given by Eq. (3.3)

$$\upsilon = \frac{1}{2\pi}\sqrt{\frac{k}{\mu}} \tag{3.3}$$

where k is the force constant of the chemical bond and μ is the reduced mass of the molecule. When a sample is exposed with IR radiation (range 200-4000 cm^{-1}), it absorbs radiation corresponding to the molecular vibration frequencies (ν) and transmits all the other frequencies. For many decades, light dispersive spectrophotometers were used in the IR spectroscopy [Bellamy, 1986]. However, now a days they are superseded by the Fourier Transform Infrared Spectrometers (FTIR). The FTIR consist of an interferometer in place of a monochromator used in

IR measurements. During the continuous scan mode, the moving mirror is continually scanned fast to generate the Fourier transform of the IR spectrum. The schematic optical design for an FTIR spectrometer is shown in Figure 3.7(a). The main components of a FTIR spectrophotometer are (i) Source, (ii) Interferometer, (iii) Sample compartment, (iv) Detector, and (v) Control Unit. In the present study, different samples are recorded using Bruker FTIR spectrometer Vertex 70v in the range of 400 to 4000 cm^{-1}. The sample preparation for FTIR measurement involves fine grinding the test sample using a mortar and pestle and its mixing with moisture-free KBr in a ratio so that optical transparency can be ensured. A thin pellet of this mixture is prepared using hydraulic press and used for measuring FTIR spectrum against the KBr reference.

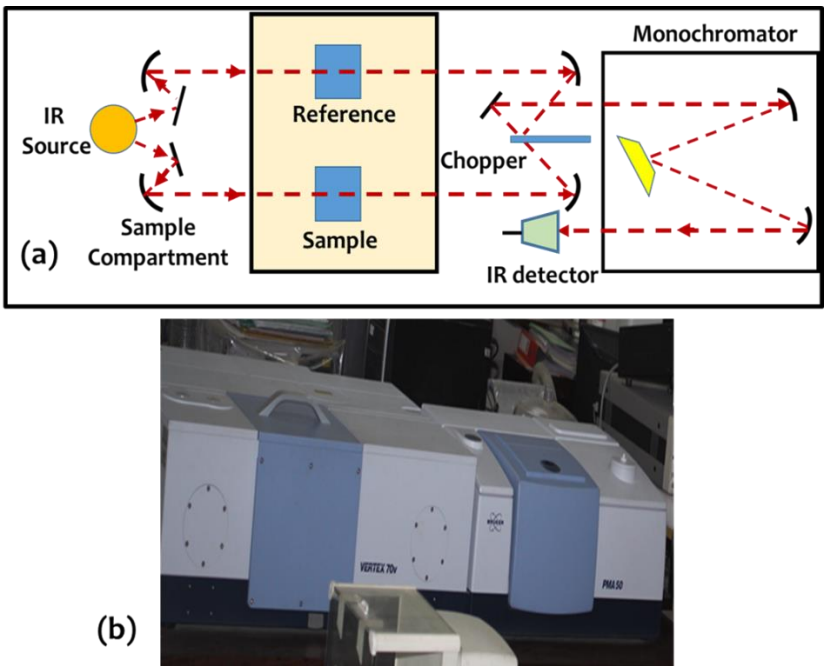

Figure 3.7 : (a) Schematic for optical design of FTIR spectrometer (b) Bruker FTIR spectrometer Vertex 70v used for IR studies

3.3.3 Vibrating Sample Magnetometer (VSM)

The vibrating sample magnetometer is the basic instrument for characterizing magnetic materials by recording their M-H hysteresis curves. VSM operates on Faraday's law of induction stating changing magnetic field produces an electric field [Foner, 1959]. VSM captures information by measuring the time rate of change of magnetic flux in the pick-up coil, caused by mechanically vibrating the magnetized sample. This instrument, schematically shown in Figure 3.8(a), employs an electromagnet, which provides the magnetizing field, a vibrator assembly to vibrate the sample during the measurements under the influence of magnetic field, and pick-up coils to generate the signal voltage due to changing flux deriving from the vibrating sample. In the VSM, a sample is connected through a non-magnetic glass or quartz rod (sample holder) to a vibration source and placed in the middle of a set of detection coils in which voltage will be induced. As the output, magnetization of the sample (in emu/g) is plotted against the applied the magnetic field (in Oe). With the help of M-H plots, the magnetic properties e.g. nature of magnetism (diamagnetism, paramagnetism, ferromagnetism and superparamagnetism), saturation magnetization and coercive field can be evaluated.

In present thesis work, the magnetic properties of the samples were investigated by using ADE model EV5 Vibrating Sample Magnetometer (VSM) at room temperature. The measurements were performed in the magnetic field range of -1.5T to +1.5T. The magnetization was calculated in emu/g from the M-H hysteresis data collected and the mass (m) of sample. The demagnetizing corrections due to sample holder and mounting rod have been considered.

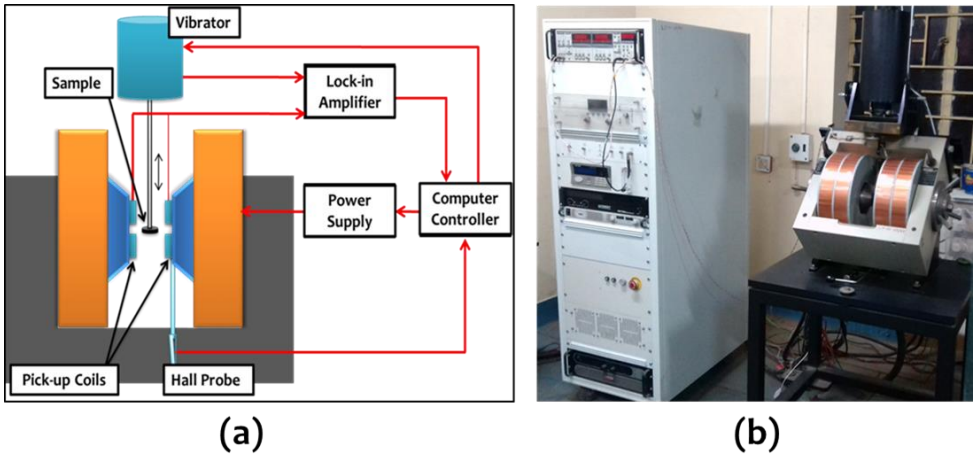

Figure 3.8: (a) Schematic for design of vibrating sample magnetometer (source: Foner, 1959) (b) ADE vibrating sample magnetometer EV5 used in M-H studies

3.3.4 Raman Spectroscopy

Raman spectroscopy is an important technique, used for investigation of structural and molecular information in terms of phonon vibrational spectrum for a material. It is based on the inelastic scattering of monochromatic light with material. The monochromatic light source is usually from a laser source. The in-elastically scattered photons have frequency shift in higher and lower side with respect to the original monochromatic frequency. This inelastic scattering of light from a material is called the Raman Effect [Schrader, 1995]. The Raman shift given by the Eq. (3.4), provides information about vibrational, rotational and other low frequency transitions in molecules. Therefore, it is a powerful tool to identify the chemical composition and structure of a material.

$$\Delta w = \left(\frac{1}{\lambda_o} - \frac{1}{\lambda_1}\right) \tag{3.4}$$

Where Δw is the Raman shift (wave number), λ_o and λ_1 are excitation and Raman wavelengths, respectively. After inelastic scattering, if the scattered light has less energy as compared to that of the incident light, the Raman shift is called Stokes shift, and when the scattered energy is higher than incident energy, the shift is called anti-Stokes shift. Figure 3.9(a) shows the optical arrangement of a typical Raman spectrophotometer. When a monochromatic light (preferably Laser) is incident on sample, the inelastic scattered Raman signals are captured by blocking the prominent Rayleigh scattered signal using notch filters. The received signals are processed through a grating monochromator prior to be recorded at the detector. In the present thesis work, Raman spectrophotometer (Make: Nomadic, Model: BaySpec, USA) was used as shown in Figure 3.9(b) with excitation wavelength of λ=532 nm, in the range of 800-1800 cm^{-1}.

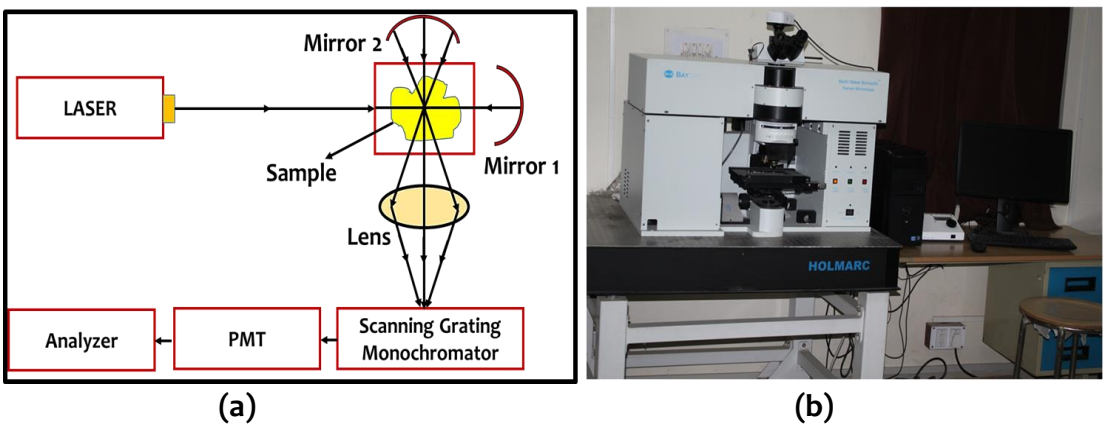

Figure 3.9 : (a) Schematic for optical design of Raman Microscope (Source: Schrader, 1995) (b) Nomadic Raman spectrophotometer (Make: BaySpec, USA) used for studies

3.3.5 Scanning Electron Microscope (SEM)

Scanning Electron Microscopy is a characterization technique to investigate the surface and grain morphology of the sample by magnified imaging using high-energy beam of electrons through scan pattern [Reimer, 1998]. When the incident electron beam interact with material sample, different particles will be generated due to transfer of energy of primary beam to sample such as Auger electrons, secondary electrons, X-ray photons, backscattered electrons and photons in visible range (cathodoluminesence). Secondary electron detector and backscattered electron detector collects these electrons that reach the detector, producing a respective signal and the corresponding image is formed on the screen or captured by CCD camera.

The block diagram of SEM is shown in Figure 3.10(a). The source of electrons in the modern instruments is heated lanthanum bromide (LaB_6) or a field emission tip. The emitted electrons are brought to a focus or cross over with the aid of a Wehnelt electrode assembly. Electron lenses are then employed to demagnify the cross-over and focus the electron probe to the surface of the sample. Two to four electromagnetic lenses are used according to gun design for focusing arrangement. It is desirable to provide the final lens with magnetic stigmator in order to correct astigmatism, which would otherwise increase the spot size. The narrow electron beam is to scan the surface of the sample with the aid of a set of x and y deflecting coils. As a result of simultaneous application of saw-tooth type wave currents to the two sets of coils, the beam can be moved along a diagonal path. The detected secondary electrons will be captured by CRT display in form of an image. In this way a complete picture of the object is displayed and can be recorded. In the present thesis, qualitative elemental analysis of the samples was done by using Oxford make Carl Zeiss EVO 18 scanning electron microscope. All non-conducting samples were sputter coated with gold before analysis.

For the elemental/compositional analysis of sample, Energy dispersive X-ray spectrometer (EDS) is used, which records the characteristic X-ray produced during interaction of primary electron beam with sample. X-ray photons that are emitted are characteristic of an element and thus, used for qualitative and quantitative detection of various elements consist in the sample. The EDS attachment (X-act) was used in conjunction with Carl Zeiss EVO18 for elemental analysis.

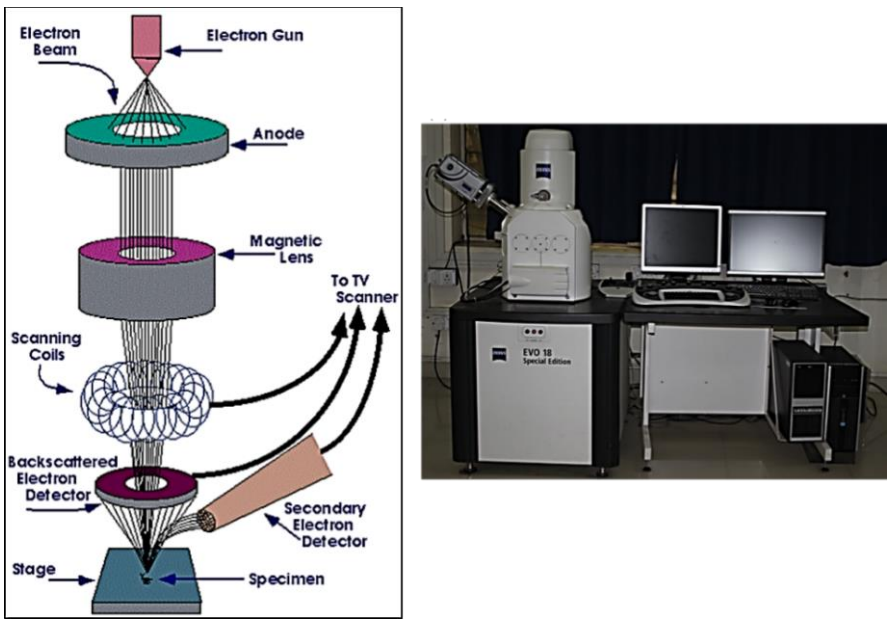

Figure 3.10: (a) Schematic block diagram of scanning electron microscope (SEM) (Source: Purdue University) (b) Carl Zeiss EVO 18 scanning electron microscope in conjunction with EDS assembly for morphological and elemental analysis

3.3.6 Transmission Electron Microscope (TEM)

Transmission electron microscopy (TEM) is a widely used characterization technique for the estimation of precise particle size, shape and crystallographic information of materials under investigation. In TEM, the high energy electron beam passes through the sample specimen, usually on the carbon grids and transmitted electron beam provides magnified image and diffraction image depending on the set-up configuration [Williams and Carter, 2009]. Figure 3.11(a) shows the schematic arrangement of TEM in both the imaging and diffraction modes. The TEM system consist of an electron gun followed by condenser lenses, which provides the confined and coherent electron beam, incident on the specially prepared thin sample slides. After passing through the sample, the transmitted electron beam is passed through objective lens used for focusing the beam to form an image. Further, with the help of intermediate and projector lenses the magnified image is obtained on the fluorescent screen.

In the diffraction TEM mode, the elastically scattered transmitted electron beam follows the Bragg's condition and objective lens creates a diffraction pattern at the back focal plane. This diffraction image is passed through a selected area aperture and projected on the screen with help of an intermediate lens assembly, also termed as Selected Area Electron Diffraction (SAED). The diffraction patterns are represented on the reciprocal space, whereas, TEM images are represented in real space. Types of diffraction patterns viz. spots, ring and diffused patterns confirm the single, polycrystalline and amorphous nature of the sample.

High-Resolution TEM (HRTEM) provides imaging of sample with atomic scale spatial resolution, by using of interference imaging of both transmitted and diffracted electron beam. In HRTEM mode no aperture is used at objective lens position. The image contrast depends on the phases on the different beams. Therefore, the imaging by HRTEM is also referred as phase contrast imaging [Smith, 2015]. In the present work, the particle morphology and SAED patterns have been obtained using a FEI TechnaiG2 model of Transmission Electron Microscope, as shown in Figure 3.11(b).

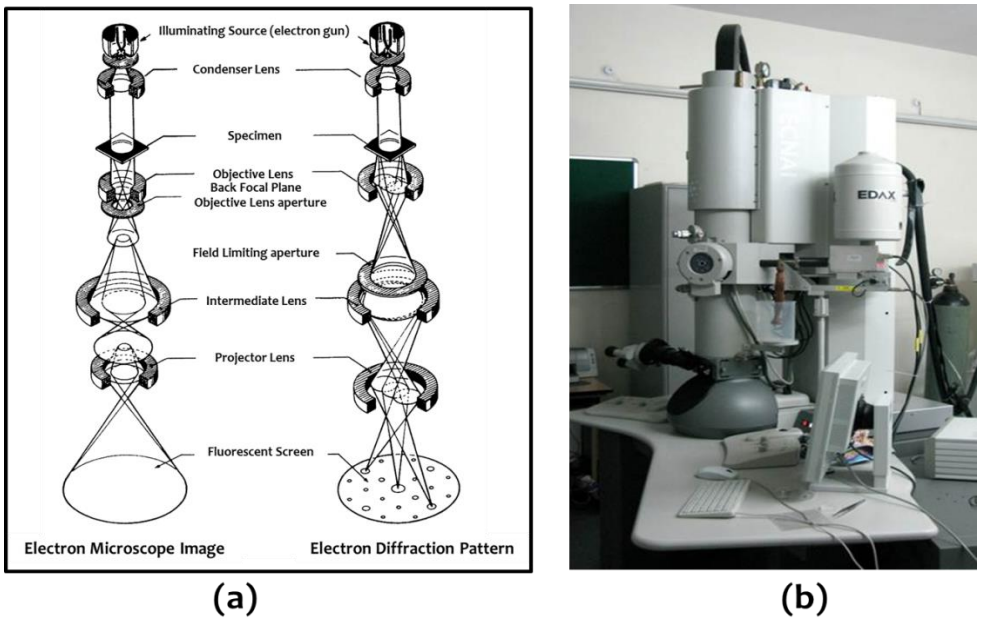

Figure 3.11: (a) Schematic block diagram of transmission electron microscope (TEM) used in imaging and diffraction mode (Source: Williams and Carter, 2009) (b) FEI Technai G2 model of Transmission Electron Microscope used for characterization

3.3.8 Superconducting Quantum Interference Device (SQUID) Magnetometer

The temperature sensitive magnetic properties, DC/AC magnetic susceptibility and other physical parameters related to magnetic flux can be evaluated using SQUID magnetometer with high accuracy. SQUID is based on the Josephson tunneling of Cooper pairs from a junction made of two superconductors separated by very thin layer of insulator. The SQUID magnetometers

composed of two Josephson junctions in parallel configuration placed in superconducting ring. The electrical current density and eventually the voltage across the contact is dependent on phase difference of superconducting wave functions (Δφ). However, the phase difference is influenced by additional magnetic flux passes through the coil [Kleiner *et al*., 2004]. As the sample moves up and down across the coil, the magnetic flux produced is captured by pick-up coils, as shown in schematic Figure 3.12(a). The magnetic flux is converted in to voltage signals and amplified by electronic circuit of SQUID magnetometer as shown in figure.

In the present study, MPMS Evercool system, from Quantum Design USA, has been utilized for recording low temperature M-H hysteresis curves and zero-field cooled (ZFC)/field cooled (FC) magnetization studies in the magnetic field range of -5T to +5T. The system is capable for magnetic measurement in the temperature range of 2K-1000K.

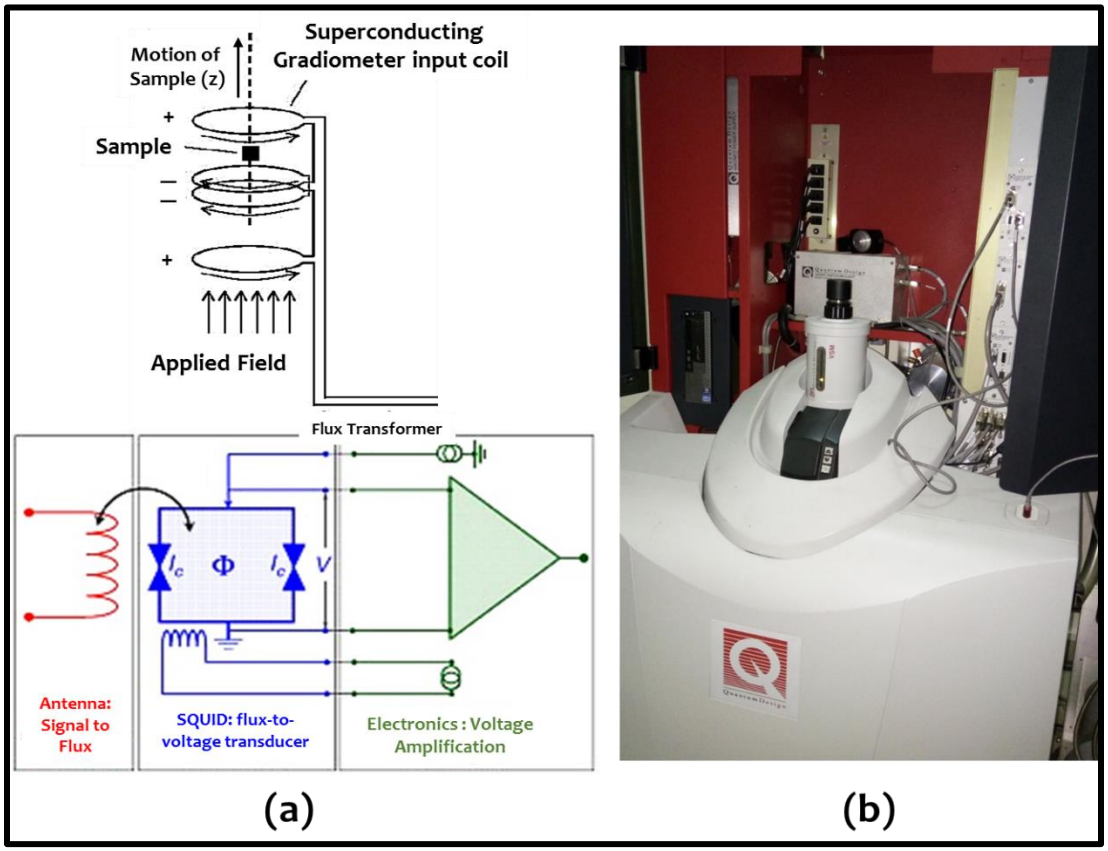

Figure 3.12: (a) Schematic block diagram of SQUID magnetometer (Black *et al*., 2006; WMI, Germany, 2015) (b) Quantum Design SQUID magnetometer MPMS Evercool used for measurement

3.3.9 Particle Size Analyzer

The average particle size of the synthesized materials was determined using particle size analyzer. Figure 3.13(a)-(b) shows the schematic of particle size analyzer, with actual photograph of Microtrac S3500 model, used for analysis. Initially, powder samples were dispersed in distilled water with the help of wetting agent Triton X-100 followed by ultra-sonication to avoid any agglomeration. Laser beam (λ=780 nm) is exposed on a sample cell containing the moving stream of suspended particle in the water. The laser beam interacts with particles and gets scattered in different possible direction over an angular distribution. The scattered laser beams are detected by photo detector arrays placed in forward directions at higher angular distributions. The photo detector arrays measure the quantity of light at specific angles. Electrical signals proportional to the measured light flux values are then processed to form a multichannel histogram of the particle size distribution. With this technique the average particle size and particles size distribution can be estimated in the range of 0.025 – 1400 μm.

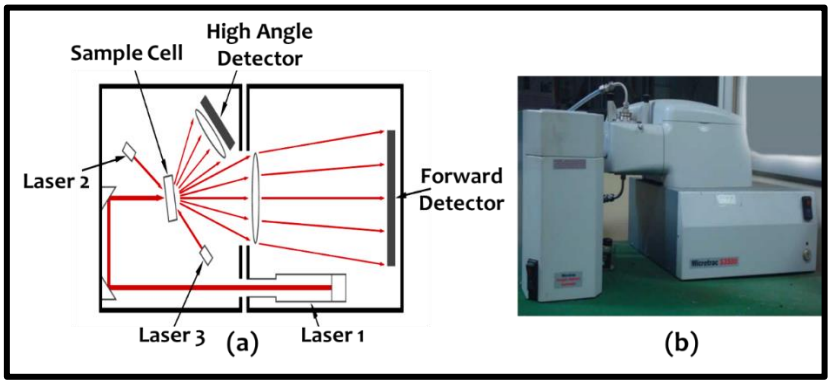

Figure 3.13 : (a) Schematic block diagram of particle size analyzer (b) Microtrac (S3500) particle size analyzer used for analysis

3.3.10 Microwave Characterization

For evaluation of complex permittivity and permeability values over GHz frequencies, MW Transmission Line Technique is being used, as it is better suited for materials with relatively high loss tangent values [Meshram *et al.*, 2003].This method is based on the measurement of the reflection and transmission scattering parameters (S parameters).These parameters are the complex ratios of the reflected/transmitted signal to the incident signal. For the evaluation of these EM parameters Vector Network Analyzer (VNA) is used to capture and analysis of data in conjunction with rectangular and circular wave guide assemblies.

3.3.7.1 Basic Principle of Measurement

The transmission line technique is an example of a class of two-port measurement technique for finding out the scattering parameters for the sample under investigation. The S-parameters description of a two-port device is shown in a flow graph notation (Figure 3.14). Where, S_{11} represents the reflected power measured at port 1, and S_{21} is the power measured at port 2, when power is incident on port 1. S_{22} and S_{12} are the corresponding parameters when power is incident upon port 2. These S-parameters are directly measurable by VNA. The complex permittivity ($\varepsilon_r^* = \varepsilon_r' - j\varepsilon_r''$) and complex permeability ($\mu_r^* = \mu_r' - j\mu_r''$) were calculated using the measured four S parameters by Nicolson-Ross-Weir (NRW) method, applicable for high lossy materials [Nicolson and Ross, 1970; Jarvis *et al.*, 2005]. In this methods, first reflection coefficient (Γ) and transmission coefficient (T) are calculated using S-parameters using Eqs.(3.5)-(3.7) [Weir, 1974]

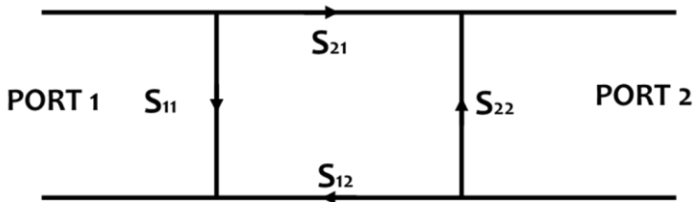

Figure 3.14: Depiction of S-parameters in two port transmission line measurement system

$$\Gamma = K \pm \sqrt{K^2 - 1} \tag{3.5}$$

$$K = \frac{S_{11}^2 - S_{21}^2 + 1}{2S_{11}^2} \tag{3.6}$$

$$T = \frac{S_{11} + S_{21} - \Gamma}{1 - (S_{11} + S_{21})\Gamma} K \tag{3.7}$$

Based on the on the calculated values of Γ and T, the materials EM parameters ε_r^* and μ_r^* can be calculated by Eqs. (3.8)-(3.9)

$$\varepsilon^* = \frac{\gamma}{\gamma_0}\left(\frac{1-\Gamma}{1+\Gamma}\right) \quad (3.8)$$

$$\mu^* = \frac{\gamma}{\gamma_0}\left(\frac{1+\Gamma}{1-\Gamma}\right) \quad (3.9)$$

Where $\gamma = \ln(1/T)/d$ and $\gamma_o = j2\pi/\lambda_o$ are wave propagation constants in medium and free space, d is the thickness of specimen and λ_o is wavelength in free space.

3.3.7.1 Vector Network Analyzer Measurement System

Vector Network Analyzer measures the magnitude and phase response of linear networks and components by comparing the incident signal with the signal transmitted by the device or reflected from its input. VNA is the instrument of choice while doing these measurements because of its swept frequency capability that enables wideband characterization in a single trace. The built in calibration and error correction functions enable the accurate measurement of these data without any tuning and matching adjustments. The block diagram of a VNA system is shown in Figure 3.15(a). Rohde and Schwarz ZVM VNA systems have been used here in conjunction with waveguide transmission line and coaxial transmission line to compute the electrical parameters of the test sample in the frequency range from 1 to 18 GHz (Figure 3.15b). The typical VNA system consists of a MW source, which is a YIG tuned crystal oscillator with synthesizer sweeper for generation of MW in the frequency range of 10 MHz-20 GHz. The reflection/transmission test sets are one-path test sets that provide automatic measurement of S-parameters. Each one of them contains a power splitter to separate the source input into reference (incident) and test (reflected and transmitted) signals. A single RF bridge or directional coupler is used to sample energy reflected from the Device Under Test (DUT)/material sample. A three channel frequency converter is included to provide RF to IF frequency conversion. The input port of the DUT is usually connected directly to the port 1 of a test set. The output port of DUT is connected to an attenuator, which in turn is connected to the single transmission return cable leading to the port 2 of test set to measure the reverse parameter in a two port device. The device must be manually reversed for the rest of the measurements. In the display and control unit, we set the desired parameters such as data display format, frequency and time domain range, averaging factor etc., before measurement and loading the respective calibration standards.

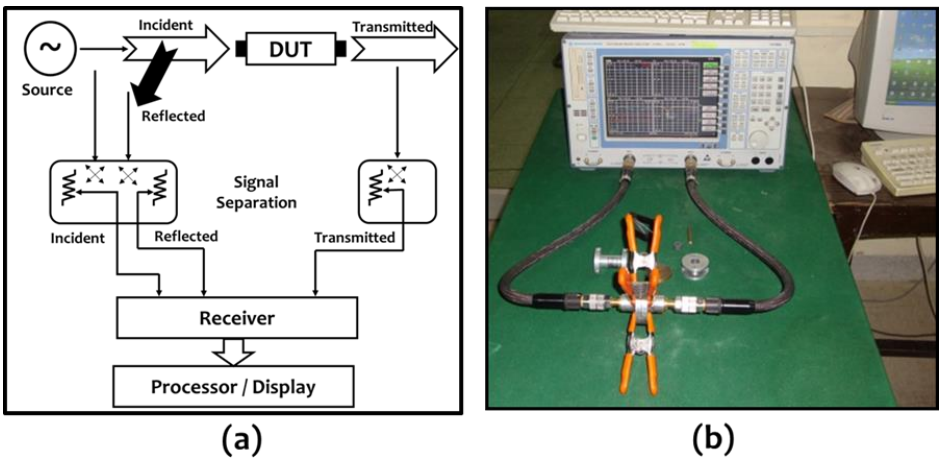

Figure 3.15: (a) Block diagram of Vector Network Analyzer (b) Rohde & Schwarz ZVM VNA system used for MW characterization

A measurement fixture is required to arrange the sample in two port configuration during the EM characterization through VNA. Here, two type of wave guide fixtures are used: (i) Rectangular fixtures (ii) Co-axial fixtures, as shown in Figure 3.16(a) and (b). In the rectangular wave guide fixtures, the samples in shape of pellets are fixed in sample holders of different dimension as per the measurement frequency bands (Fig. 3.16c). The sample holder interfaces to the VNA test-port cables through coaxial-to-waveguide adaptors. Table 3.2 shows the typical

dimensions of rectangular sample holders and their respective frequency band width for R, S, G, J, X and Ku-bands based on the different cut-off wave length of rectangular wave guides for each band.

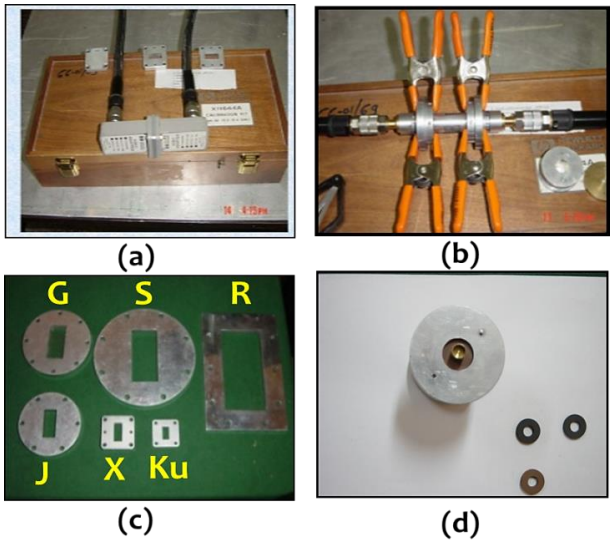

Figure 3.16: (a) Rectangular wave guide fixture (b) Co-axial wave guide fixture (c) Rectangular sample holders for R, S, G, J, X and Ku bands (d) Co-axial sample holder

Table 3.2 : List of dimension of rectangular wave guide sample holders for different MW frequency bands

Frequency Band	Frequency range (GHz)	Waveguide inside Dimensions (mm)	
		Length	Width
R	1.7-2.6	108.36	54.18
S	2.6-3.95	72.14	34.04
G	3.95-5.85	47.55	22.15
J	5.85-8.2	34.85	15.80
X	8.2-12.4	22.86	10.16
Ku	12.4-18	15.80	7.90

The waveguide method imposes some limitations on the measurements due to its frequency band constraints. The sample has to be measured in six different bands to cover the entire frequency range 2-18 GHz. Moreover, as the frequency goes towards lower band side, the sample size has to be increased and it is very difficult to prepare a large sample in rectangular shape of this size with a required precision. Therefore, for low frequency region coaxial transmission line method is more suitable. Since the cutoff frequency for this method is zero, hence there is no restriction of band size in this method and broad band frequency measurements are possible in a single set of measurement. Model M14T material measurement fixture has been used in conjunction with Rohde & Schwarz systems as shown in Figure 3.16(d). The sample holders are 50 Ω coaxial 7 mm bidless air lines with 6.21 mm inner diameter and 14.27 mm outer diameter dimensions. Samples are prepared in an annular shape. Measurements using this method were carried out in the frequency range 1-6 GHz. Therefore, the co-axial transmission line measurement is advantageous for low frequency measurements of Ni-Zn spinel ferrite samples without making large dimension pellets for each frequency band in the range of 1-6 GHz. The obtained complex permittivity and permeability data were used in computing the thickness dependent reflection loss (R.L.) characteristics of absorbers using in-house developed MATLAB program.

...